Oscillatory surface dichroism of the insulating topological insulator Bi_2Te_2Se

M. Neupane,[1] S. Basak,[2] N. Alidoust,[1] S.-Y. Xu,[1] Chang Liu,[1] I. Belopolski,[1] G. Bian,[1] J. Xiong,[1] H. Ji,[3] S. Jia,[3] S.-K. Mo,[4] M. Bissen,[5] M. Severson,[5] H. Lin,[2] N. P. Ong,[1] T. Durakiewicz,[6] R. J. Cava,[3] A. Bansil,[2] and M. Z. Hasan[1,7,*]

[1]*Joseph Henry Laboratory and Department of Physics, Princeton University, Princeton, New Jersey 08544, USA*

[2]*Department of Physics, Northeastern University, Boston, Massachusetts 02115, USA*

[3]*Department of Chemistry, Princeton University, Princeton, New Jersey 08544, USA*

[4]*Advanced Light Source, Lawrence Berkeley National Laboratory, Berkeley, California 94305, USA*

[5]*Synchrotron Radiation Center, Stoughton, Wisconsin 53589-3097, USA*

[6]*Condensed Matter and Magnet Science Group, Los Alamos National Laboratory, Los Alamos, New Mexico 87545, USA*

[7]*Princeton Center for Complex Materials, Princeton University, Princeton, New Jersey 08544, USA*

(Received 30 July 2013; published 21 October 2013)

Using circular dichroism-angle resolved photoemission spectroscopy, we report a study of the effect of angular momentum transfer between polarized photons and topological surface states on the surface of the insulating topological insulator Bi_2Te_2Se. The photoelectron dichroism is found to be strongly modulated by the frequency of the helical photons including a dramatic sign flip. Our results suggest that the observed dichroism and its sign flip are consequences of strong coupling between the photon field and the spin-orbit nature of the Dirac modes on the surface. Our studies reveal the intrinsic dichroic behavior of topological surface states and point toward the potential utility of bulk insulating topological insulators in opto-spintronics device applications.

DOI: 10.1103/PhysRevB.88.165129 PACS number(s): 71.20.−b

I. INTRODUCTION

While the basic electronic structure and spin-momentum locking of topological insulators have been studied using surface sensitive probes such as angle-resolved photoemission spectroscopy and scanning tunneling microscopy[1–19], much remains to be discovered regarding their critical and strong response to light, electric, or magnetic fields. Such perturbations can selectively couple to different aspects of the surface wave function. The full wave function of the topological surface states (TSSs) is known to feature not only strong spin-orbit coupled texture but also its variation and modulation from layer to layer due to its finite penetration into the bulk.[13,20] Therefore, it is of critical importance to understand the nature of electron-photon scattering process in the TSS. It is commonly believed that the single-frequency dichroic signal reveals the spin (and/or orbital) texture of the material and also controls the photocurrent.[9–11,13–16] However, in real materials, this apparently simple control process is further complicated by multiple factors including the presence of bulk bands at the Fermi level leading to surface bulk hybridization, quantum well formation and surface-bulk scattering thus masking the intrinsic response. Predictable control of the topological surface states has not yet been achieved.

Optical circular dichroism has been extensively applied to study magnetic materials before.[21–23] Recently circular dichroism-angle resolved photoemission (CD-ARPES) is used to study the surface states of topological insulators.[24–26] In order to understand the intrinsic dichroic behavior of topological surface states it is important to study the effect of angular momentum transfer between the polarized photons and the surface states as a function of photon frequency and polarization in a highly bulk insulating topological insulator class where the Fermi level lies within the bulk band gap and cuts across the topological surface states only. We carried out circular dichroism-angle resolved photoemission measurements on Bi_2Te_2Se (BTS221), a recently realized bulk resistive topological insulator (more than 6 Ω cm). The BTS221 sample shows much better insulating characteristics compared to Bi_2Te_3 or Bi_2Se_3, with an in-gap Fermi level, and is thus ideal for exploring the real origin of dichroic effects without complications related to interaction between the bulk and surface states. This is not possible in Bi_2Te_3.[26] We report that the intrinsic dichroism is strongly modulated by the frequency of photons including a dramatic sign flip, which further undergoes magnitude oscillations. Our results suggest a lack of unique experimental correspondence between the dichroism and spin-texture chirality (right or left handedness) for a specific photon frequency. We present theoretical calculations accounting for the Dirac-electron and helical-photon interaction and show that the sign flip and the magnitude modulation in dichroism are consequences of the combined effect of strong coupling between the photon helicity and the spin-orbit texture of the massless Dirac modes and the projection of the multiple orbital-textures within the effective skin depth of the topological surface states.

II. METHODS

Single crystalline samples of topological insulators were grown using the Bridgman method, which is detailed elsewhere.[27–29] ARPES measurements for the low-energy electronic structure were performed at the Synchrotron Radiation Center (SRC), Wisconsin, equipped with high efficiency VG-Scienta SES2002 electron analyzers, using the U9 VLS-PGM beam, and the Advanced Light Source (ALS), California, using BL10 equipped with high-efficiency R4000 electron analyzers. The polarization purity is better than 99% for horizontal polarization (HP) and better than 80% for right circularly polarized (RCP) and left circularly polarized (LCP) light. Samples were cleaved *in situ* and measured at 20 K in a vacuum better than 1×10^{-10} torr. Energy and momentum resolution were better than 15 meV and 1% of the surface Brillouin zone (BZ), respectively. We theoretically calculate the CD

response on the surface of BTS221, where the electronic structure of BTS221 is modeled by the tight-binding theory with the parameter fitted by the GGA results. The ARPES matrix element effects is considered in the electron-photon scattering process.

III. RESULTS AND DISCUSSION

A. Bulk insulating Bi_2Te_2Se

The crystalline symmetry, the cleavage plane (Te layer) and sample characterization for BTS221 are shown in Fig. 1. It is believed that the reduction in the bulk conductivity is possible in BTS221 due to the confinement of Se atoms within the central layer, which likely suppresses the Se vacancy generation as well as reduces the antisite defects between Bi and Te atoms. Comparative resistivity profiles show a significant degree of bulk insulation in BTS221 with respect to prototype materials such as Bi_2Te_3 and Bi_2Se_3. Based on the period of oscillations in high-field transport, we obtain an averaged two-dimensional (2D) carrier concentration $n_s \sim 1.7 \times 10^{12}$ cm^{-2} and hence a Fermi momentum of $k_F \sim 0.047$Å^{-1}. Applying a standard Dingle analysis to the SdH amplitudes, we infer a surface mobility $\mu_s = 2{,}800$ cm^2/Vs and a Fermi velocity $v_F = 6 \times 10^5$ m/s in our samples.[30] The nonconducting behavior of the bulk and the in-gap Fermi level in our samples reduce the possibility of interaction of bulk and surface states, which is also evident from the high degree of surface state contribution to transport typically seen in the quantum oscillation data.[30] These results are in qualitative agreement with conventional band-structure measurements of BTS221.[18,19] BTS221 samples thus provide an ideal platform to explore the intrinsic CD effect theoretically expected from the topological surface states, which is not possible with metallic Bi_2Te_3 TI.[26]

B. Experimental observation of oscillating circular dichroism

The ARPES dispersion maps of surface states for BTS221 are shown in Fig. 2(a) while the experimental geometry used for the CD measurements is shown in the inset of Fig. 4(a). The sample surface is parallel to the *XY* plane and circularly polarized photons (spiral arrow) propagate in the *XZ* plane at an angle (θ) of 50° to the sample surface normal. The chemical potential is found to lie within the bulk band gap cutting across the TSS only. A nearly isotropic surface Fermi surface without any significant hexagonal deformation is seen, which suggests that this system can be thought of as a material realization of a nearly ideal Dirac Fermion gas near the native chemical potential. This also indicates a near absence of interaction between bulk and surface states [in contrast to the hexagonally warped lower Dirac cone of Bi_2Te_3 shown in the inset of Fig. 1(b)[31]]. The Dirac node in BTS221 is found to be nearly buried within the bulk valence band, which makes the surface state in the lower cone degenerate with bulk bands. As a result, the intrinsic CD effect associated with the lower Dirac cone cannot be clearly disentangled from the bulk. We therefore focus on the detailed CD behavior of the upper Dirac band.

A clear surface state CD response on the photoelectron signal from the upper Dirac cone is observed where the $+k$ Dirac branch is positive and the $-k$ Dirac branch is negative in CD intensity (Fig. 2). The magnitude of the CD response signal defined as $I_{CD} = (I_{RCP} - I_{LCP})/(I_{RCP} + I_{LCP})$ is observed to be about 20% for incident photons with an energy of 18 eV in BTS221 for electrons with binding energy of about 150 meV, well below the chemical potential. This CD behavior is qualitatively consistent with previous work on other TIs such as $Cu_xBi_2Se_3$[12] and Bi_2Se_3.[13,15,32] Previously such CD response has been used to derive the details of spin texture and chirality under the assumption that the response measured at a single frequency qualitatively samples the complete surface state wave function properties. In a multiorbital system where the surface state penetrates more than the very top layer a single photon energy may not capture the full details of the wave function. Indeed, analogously measured CD response but for the 23 eV photons shows, in our data Fig. 2(b), a momentum space reversal of CD sign per Dirac band, namely, the $+k$ Dirac branch is negative whereas the $-k$ Dirac branch is

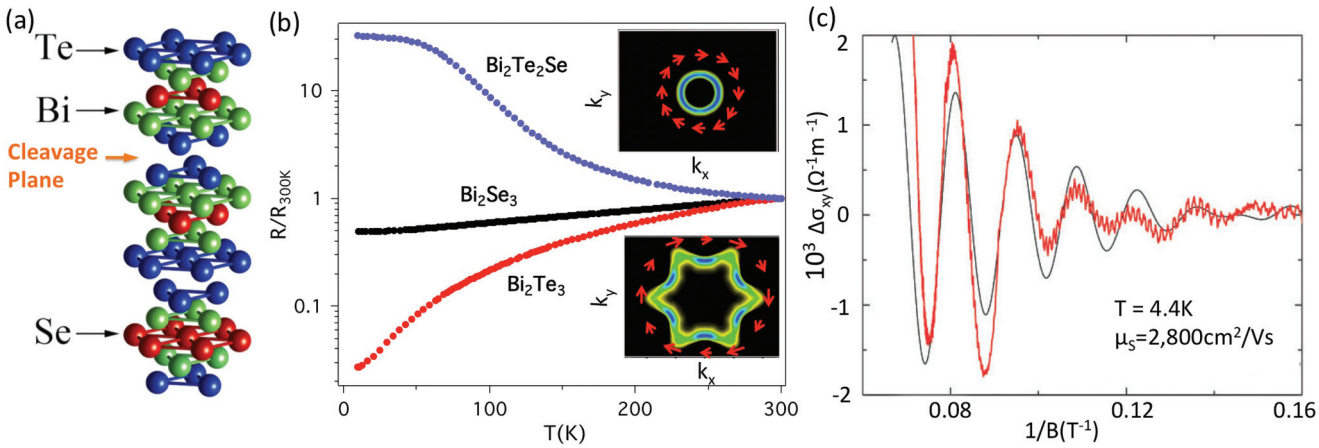

FIG. 1. (Color online) (a) Crystal structure of BTS221. Red, green, and blue circles represent the Se, Bi, and Te atoms, respectively. (b) Normalized in-plane resistivities (R/R_{300}) plotted as a function of temperature (T) for BTS221. The resistivity profiles of Bi_2Se_3 and Bi_2Te_3 are added for comparison. Insets show the Fermi surface plots for BTS221 (upper panel) and Bi_2Te_3 (lower panel). Arrows around the FS represent the in-plane spin texture. (c) Shubnikov-de Haas oscillation measurements on the topological surface of BTS221 (see Ref. 30 for details).

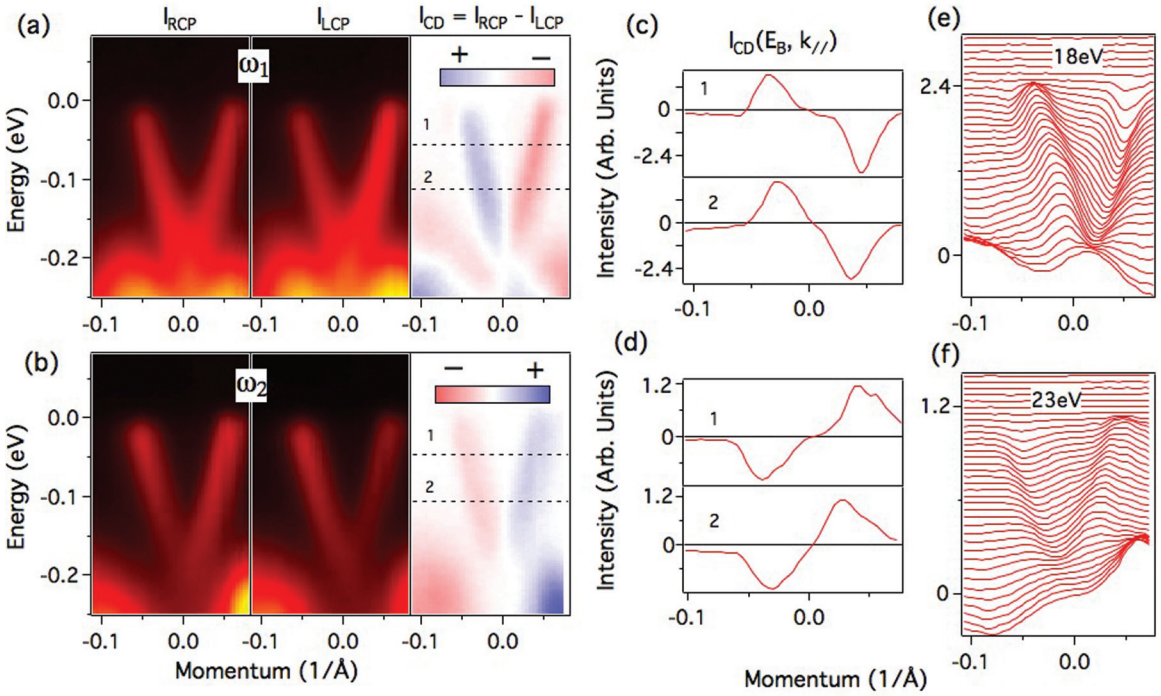

FIG. 2. (Color online) (a) High-resolution ARPES measurements of Bi_2Te_2Se for right circularly polarized (RCP) light, left circularly polarized (LCP) light and the photoelectron circular dichroism ($I_{RCP} - I_{LCP}$) measured with photon energy $\omega_1 = 18$ eV. (b) Analogous measurements as in (a) for photon energy $\omega_2 = 23$ eV. These spectra are measured along the $\bar{\Gamma} - \bar{M}$ high symmetry momentum-space cut. (c) The measured CD values for binding energies of 50 meV and 100 meV as marked on the I_{CD} plot of (a) by black dashed lines and denoted by numbers 1 and 2. (d) Similar measurements as (c) for (b). (e) and (f) The momentum distribution curves of CD spectra for 18 eV and 23 eV photons, respectively.

positive. The reversal of CD between 18 and 23 eV is also seen in our systematic measurements of the momentum distribution profiles [Figs. 2(c)–2(f)]. We further study the CD response of these samples with photons of intermediate energies to study the functional dependence on photon frequency or energy. We present angle-resolved photoemission spectroscopy (ARPES) dispersion maps (raw data) measured using right circularly polarized light (RCP) and left circularly polarized light (LCP) with different photon energies for the Bi_2Te_2Se (BTS221) sample in Fig. 3. The top row shows the ARPES spectra using RCP light, which shows that the intensity of the left branch of the upper Dirac cone first decreases and then increases with respect to the right branch of the cone in passing from photon energy 19 eV to 31 eV. The opposite effect is observed for the spectra measured using LCP light (see middle panels). As a result, the oscillative nature of the surface circular dichroism is observed (bottom panels of Fig. 3). It is important to note that the CD values at low photon energies is $\sim 20\%$ but for photon energies of 28 eV and 29 eV they reach ~ 70 %. A weaker CD response is observed at photon energy of 20 eV, where the sign of the CD is about to flip. Larger CD values are observed between photon energies of 23 eV and 24 eV through which a sign flip of CD is observed. Figure 4 summarizes the CD response, magnitude and sign, in BTS221 within photon energies from 20 to 31 eV. We found that the reversal of CD between 18 eV and 23 eV is in fact a part of the full oscillation profile.

In order to further check the generality of our observation, we perform surface CD-ARPES measurements on two other TI systems, namely $Bi_{1.4}Sb_{0.6}Te_{1.5}S_{1.5}$ (BiSbTeS) and the prototype Bi_2Te_3. It is known from ARPES measurements that $Bi_2Te_{1.5}S_{1.5}$ is a single Dirac cone topological insulator in the tetradymite family where antimony is usually substituted in place of Bi in the $Bi_2Te_{1.5}S_{1.5}$ lattice to systematically tune the chemical potential.[19,27] We present CD response of the surface of BiSbTeS, where dispersive topological surface states are observed [Fig. 5(a)]. Our BiSbTeS sample is slightly *n* type, the Fermi level is observed to be located in the conduction band, which is about 250 meV above the Dirac point. The flipping of the CD sign is observed in the spectra measured at 19 eV and 23 eV. It is also important to note that the bulk conduction bands at 19 eV is suppressed as compared to that of data taken with 23 eV photons. Since the bulk conduction bands are not degenerate with the surface states, a clear contrast in CD signal is observed.

Furthermore, we have carried out similar measurements on the surface of Bi_2Te_3, which is a large spin-orbit-induced indirect bulk band gap semiconductor whose surface is characterized by a hexagonal surface state.[8] The measured Bi_2Te_3 sample is slightly *n* doped, where the chemical potential is in conduction bands, about 180 meV from the Dirac point (not seen in the data due to the photon-energy-related matrix element effect). The Dirac point is buried in the bulk valence band unlike Bi_2Se_3. It is worth noting that the effect of CPR and CPL light is stronger in the spectra taken with 31 eV photons in which an intense upper Dirac cone is observed for positive and negative wave vectors using CPR and CPL light,

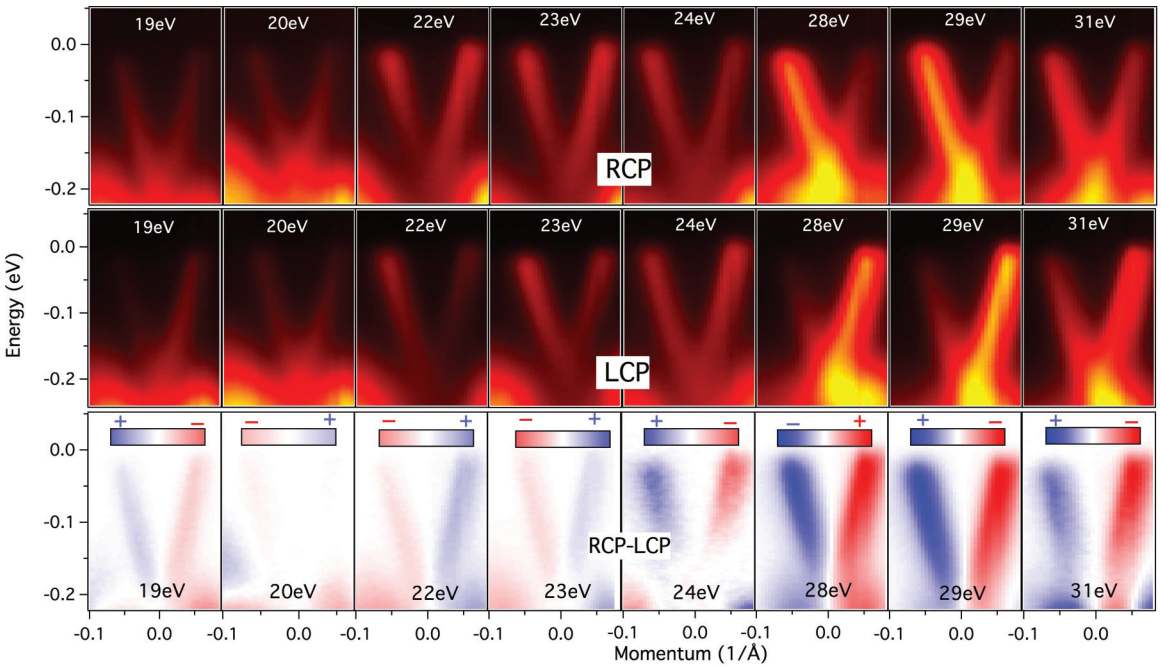

FIG. 3. (Color online) ARPES data demonstrating oscillations in the CD signal. Raw data of high-resolution ARPES measurements of BTS221 for 19 eV, 20 eV, 22 eV, 23 eV, 24 eV, 28 eV, 29 eV, and 31 eV with right circularly polarized (RCP) light (top row), with left circularly polarized (LCP) light (middle row), and the circular dichroism (RCP-LCP) (bottom row). These plots provide a direct visualization of the oscillatory behavior of the surface CD signal. The measured photon energies are noted on the spectra.

respectively. Our CD-ARPES results on the surface states of the upper Dirac cone of Bi_2Te_3 system measured with 29 eV and 31 eV photons [Fig. 5(b)] also exhibit the flipping of CD sign, which is consistent with the recent report.[26] Our results indicate that the intrinsic CD of the topological surface states is strongly modulated with photon energy and the existence of the sign-flip suggests that the CD signal can not be a straightforward reflection of the spin texture of the initial ground

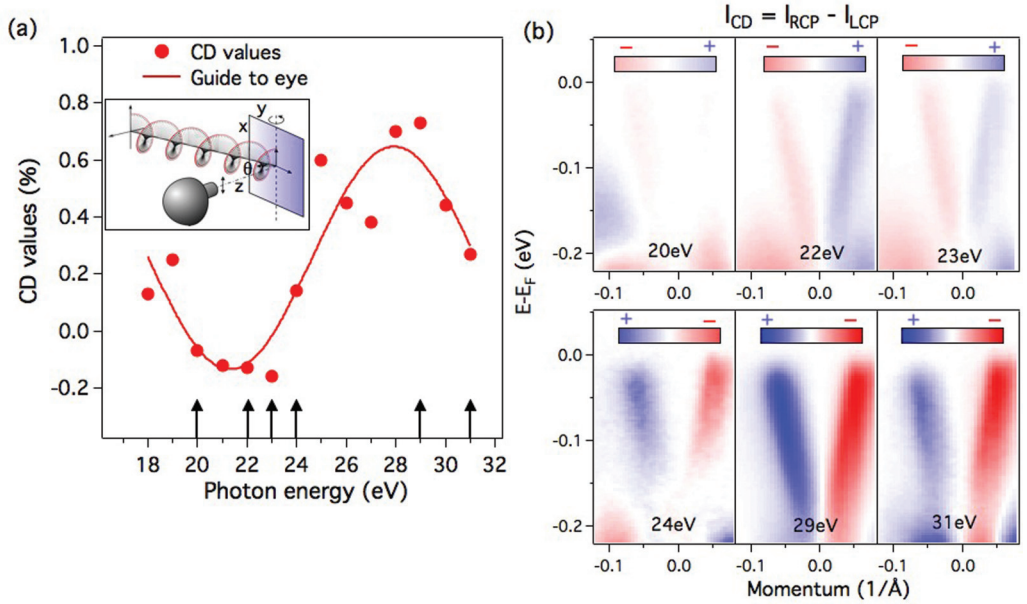

FIG. 4. (Color online) (a) The measured CD values are plotted as a function of photon energy. The photoelectron CD value is estimated as $I_{CD} = (I^+ - I^-)/(I^+ + I^-)$ for data taken with momentum $k \sim -0.05$ Å^{-1} and binding energy ~ 100 meV. Arrows represent the photon energies of representative CD-ARPES spectra presented in (b). Inset shows the geometry of the ARPES measurement (see text for details). (b) ARPES plots of the circular dichroic photoemission with various photon energies. The corresponding photon energies are noted on the plots. The spectra taken with 20–23 eV exhibit negative CD values (top row) while it is taken with 24–31 eV exhibit positive CD values (bottom row).

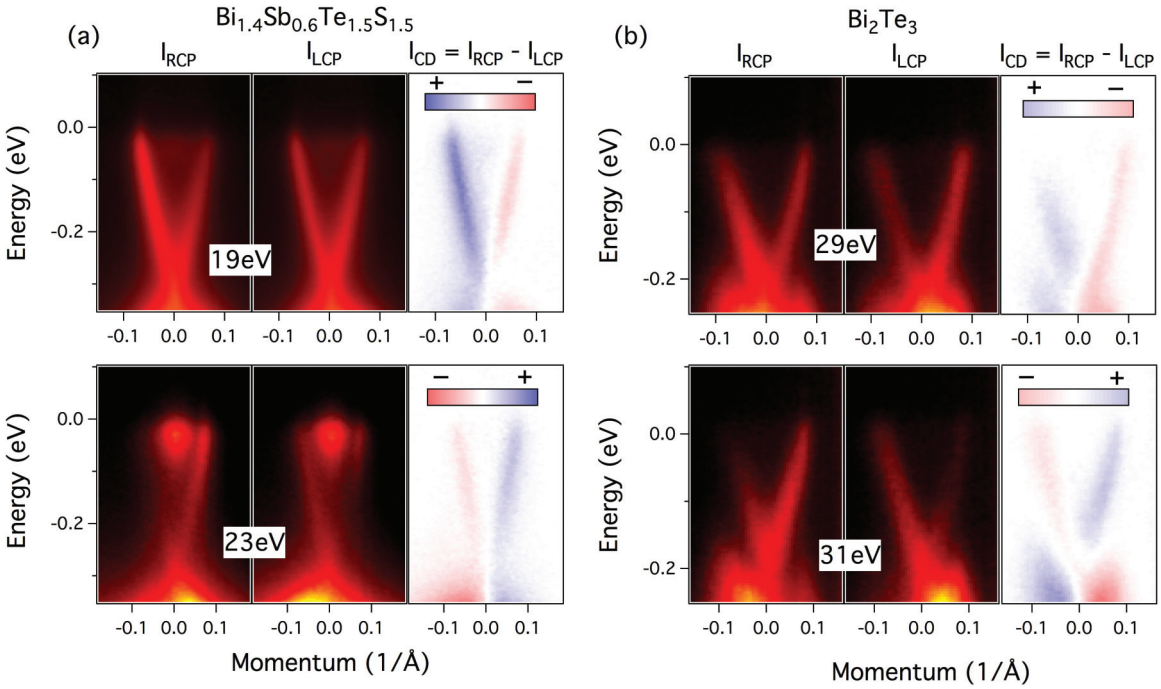

FIG. 5. (Color online) Oscillatory dichroism in other TI systems. (a) ARPES measurements of $Bi_{1.4}Sb_{0.6}Te_{1.5}S_{1.5}$ for right circularly polarized (RCP) light, left circularly polarized (LCP) light and the circular dichroism (RCP-LCP). The top row spectra are measured with photon energy 19 eV while the bottom row spectra are measured with photon energy 22 eV. (b) ARPES measurements of Bi_2Te_3 for right circularly polarized (RCP) light, left circularly polarized (LCP) light and the circular dichroism (RCP-LCP). The top row spectra are measured with photon energy 29 eV while the bottom row spectra are measured with photon energy 31 eV. These results suggest that the oscillatory behavior of the CD response is a more general property of topological insulators.

state.[26,33,34] These systematics imply that the CD modulation and sign-flip behavior is likely to be a general property of the topological surface states independent of the materials family.

C. Theoretical origin of the oscillating nature of dichroism

To explain the modulation depth and sign flip, we calculated circular dichroism in ARPES starting from an DFT(GGA) based Hamiltonian for BTS221, which takes care of crystal symmetry and includes spin-orbit coupling. The Hamiltonian for a system with spin-orbit coupling is given by

$$H_{SO} = \frac{p^2}{2m} + V(\mathbf{r}) + \frac{\hbar^2}{4m^2c^2}\sigma \cdot (\mathbf{p} \times \nabla V), \qquad (1)$$

where $\mathbf{p}$ is the momentum operator, $V(\mathbf{r})$ is the crystal potential and $\sigma = (\sigma_x, \sigma_y, \sigma_z)$ is the spin of electrons. After coupling with a photon with vector potential $\mathbf{A}$, the momentum operator becomes $\mathbf{p} \rightarrow \mathbf{p} - e\mathbf{A}$. The Hamiltonian becomes

$$H_{SO}(\mathbf{A}) = H_{SO} - H_{\text{int}}, \qquad (2)$$

where the interaction with photon is

$$H_{\text{int}} = \frac{e}{m}\mathbf{A} \cdot \mathbf{p} - \frac{\hbar e}{4m^2c^2}\mathbf{A} \cdot (\nabla V \times \sigma). \qquad (3)$$

Assuming circularly polarized light propagating along the z axis with a vector potential $\mathbf{A} = A_0(\hat{\mathbf{x}} \pm i\hat{\mathbf{y}})$, where the $+$ and $-$ signs refer to right and left circularly polarized light, respectively, the Hamiltonian in Eq. (3) becomes

$$H_{\text{int}}^{\pm} = \frac{eA_0}{m}(p_x \pm ip_y) - \frac{\hbar eA_0}{4m^2c^2}\left(\pm iE_{cf}^z S_{\pm} + \left(E_{cf}^y \mp iE_{cf}^x\right)S_z\right), \qquad (4)$$

where $S_{\pm} = \sigma_x \pm i\sigma_y$ are the spin raising and lowering operators, respectively, up and down spins being eigenkets of $S_z = \sigma_z$ and $\mathbf{E}_{cf} = -\nabla V = (E_{cf}^x, E_{cf}^y, E_{cf}^z)$ is the crystal field treated here as a constant. The photoemission matrix element is $M_{\pm} = \langle f|H_{\text{int}}^{\pm}|i\rangle$ where $|i\rangle$ and $|f\rangle$ are initial and final states, respectively. The circular dichroism is obtained by taking the difference between photocurrents due to right and left circular polarized light,

$$I_{CD}(\mathbf{k_f}, \mathbf{k}, E) \propto \left(|M_+(\mathbf{k_f})|^2 - |M_-(\mathbf{k_f})|^2\right)\mathcal{W}(\mathbf{k}, E), \qquad (5)$$

where $\mathcal{W}(\mathbf{k}, E) = -\frac{1}{\pi}\text{Im}G(\mathbf{k}, E)$ is the spectral function and $G(\mathbf{k}, E)$ is the Green's function associated with the initial-state electrons with momentum $\mathbf{k}$ and energy E and $\mathbf{k_f}$ is the final-state electronic momentum. The initial state is expanded into atomic orbital (nlm) of the ith atom in the unit cell at position $\mathbf{R_i}$, $|i\rangle = R_{nl}(r)Y_{lm}(\theta,\phi)|\chi\rangle_{nlm}$ where the spin function is $|\chi\rangle_{nlm} = \chi_{nlm,\uparrow}|\uparrow\rangle + \chi_{nlm,\downarrow}|\downarrow\rangle$, $|\uparrow\rangle$ and $|\downarrow\rangle$ being the spin eigenstates for the quantization axis along the z direction. Note that these initial states are the topological surface states, which are obtained by using a Green's function renormalization-decimation technique for a semi-infinite slab of BTS221.[35] The final state is approximated as spin-degenerate free electron state with momentum $\mathbf{k_f}$.

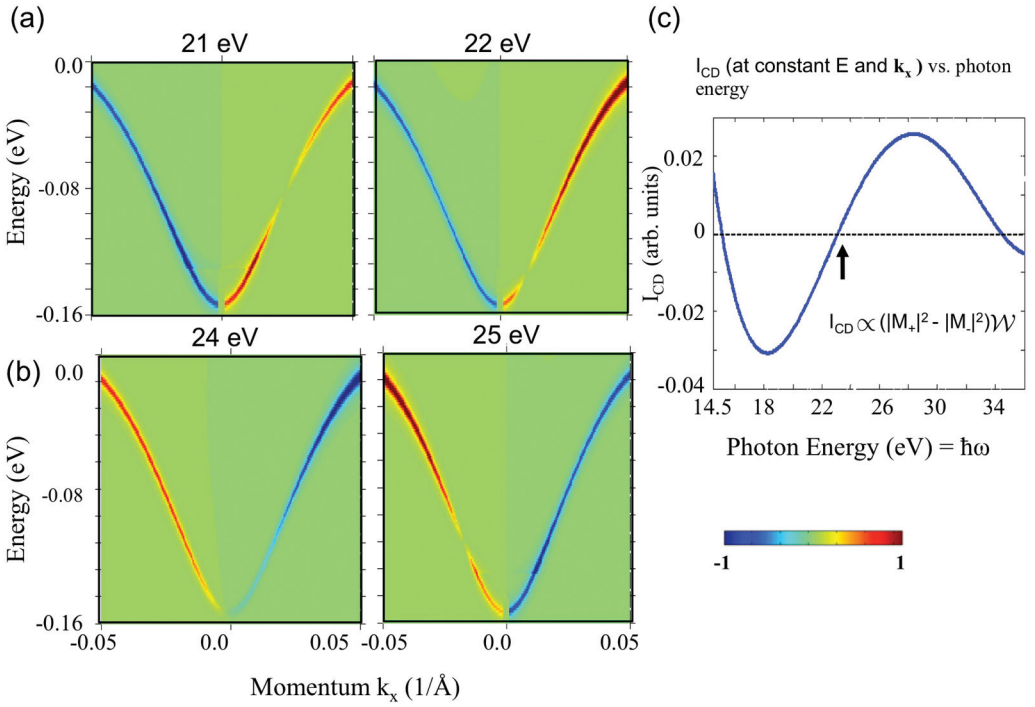

FIG. 6. (Color online) Model calculations are carried out for photon energies of (a) 21 eV and 22 eV, and (b) 24 eV and 25 eV. The change in the sign of CD can be observed by comparing spectra shown in (a) and (b). (c) The theoretically calculated I_{CD} at constant k_x and E as a function of photon energy. The black arrow indicates the photon energy value where flipping of CD sign is expected in our theoretical model for BTS221.

The final forms of M_+ and M_- are the following:

$$M_+ = \sum_{i,nlm}(-i)^l e^{i\mathbf{k_f}\cdot\mathbf{R_i}} F_{nl}(k_f) Y_{lm}(\theta_{k_f},\phi_{k_f}) \times \left(i E^z_{cf}\chi_{nlm,\downarrow} + \left(E^y_{cf} - i E^x_{cf}\right)\chi_{nlm}\right); \quad (6)$$

$$M_- = \sum_{i,nlm}(-i)^l e^{i\mathbf{k_f}\cdot\mathbf{R_i}} F_{nl}(k_f) Y_{lm}(\theta_{k_f},\phi_{k_f}) \times \left(-i E^z_{cf}\chi_{nlm,\uparrow} + \left(E^y_{cf} + i E^x_{cf}\right)\chi_{nlm}\right), \quad (7)$$

where $F_{nl}(k_f) = \int r^2 dr j_l(k_f r) R_{nl}(r)$ is the form factor associated with the atomic orbital (nlm), j_l is a spherical Bessel function, and $R_{nl}(r)$ is the the radial part of the atomic wave function, Y_{lm} is the spherical harmonic for the angular variables of $\mathbf{k}_f$ and $\chi_{nlm} = \chi_{nlm,\uparrow} - \chi_{nlm,\downarrow}$.

We emphasize that we use the three-step model of photoemission to determine $M_\pm(\mathbf{k_f})$ in which the photoemission process is broken down into three independent and sequential steps: (i) excitation of the bulk electrons, (ii) transport of the excited electrons to the surface, and (iii) their escape into the vacuum. This model allows a straightforward disentanglement of various factors controlling the observed spectral features by considering the microscopic processes at play. Whereas the alternate option, the one-step model of photoemission, treats the photoemission process as a single coherent event and it is often difficult to adduce physical microscopic insight into the origin of spectral features resulting from this model.[26]

Combining Eqs. (5), (6), and (7) we get the final form of I_{CD} as the following:

$$I_{CD}(\mathbf{k_f},\mathbf{k},E) \propto \mathcal{W}(\mathbf{k},E)\sum_{i,nlm}|\mathcal{J}_{i,nlm}(k_f)|^2[a(|\chi_{nlm,\uparrow}|^2 - |\chi_{nlm,\downarrow}|^2) + b\mathrm{Im}(\chi^*_{nlm,\uparrow}\chi_{nlm,\downarrow})], \quad (8)$$

where a and b are constants, which depend on E_{cf} and $\mathcal{J}_{i,nlm}(k_f) = (-i)^l e^{i\mathbf{k_f}\cdot\mathbf{R_i}} F_{nl}(k_f) Y_{lm}(\theta_{k_f},\phi_{k_f})$. Note that the above equation is a simplified form of I_{CD}, which holds when there is one significant orbital in each quintuple layer, meaning (nlm) has one set of values. In our calculation we consider all five atoms and associated p orbitals in one QL as the basis of our Hamiltonian and therefore I_{CD} has a more complicated form due to the interference between orbitals in the same atom and in different atoms. The tight-binding paramaters are obtained by fitting to the GGA band structure of BTS221. The values of work function (W) and inner potential (V_0) obtained from first-principles calculations are 4.8 eV and 7.2 eV, respectively.

The above result shows how the circularly polarized light couples to the spin of topological surface states via a spin-orbit interaction. The spin-dependent part of I_{CD} is the intrinsic property of the material itself and can not vary with the photon energy. Therefore, the oscillation with photon energy should be originated from the term $\mathcal{J}_{i,nlm}(k_f)$, which is the coupling between the initial and final states via electron-photon interaction, and from the previously discussed momentum and energy conservation arguments we find how $\mathcal{J}_{i,nlm}(k_f)$

depends on photon energy. In Figs. 6(a) and 6(b) we plot the theoretical CD signal for two sets of photon energies and the CD sign flip is reproduced. The first sign flip is observed in between 23 and 24 eV photon energy. In spite of the approximations within the three-step model of photoemission, we obtained a close agreement between the theory and the experiment. In Fig. 6(c) we plot the CD intensity as a function of photon energy at a constant energy and momentum and it reveals an oscillatory nature about zero. This sign flip is a manifestation of the oscillatory nature of $\mathcal{J}_{i,nlm}(k_f)$. The structure factor $e^{i\mathbf{k_f}\cdot\mathbf{R_i}}$ also indicates that the surface states may have a spatially dependent orbital mixing and it can be probed by varying the perpendicular component of the Bloch wave vector, $k_{f\perp}$ through its dependence on photon energy. As a result, the CD of the surface states could have a nontrivial dependence on the $k_{f\perp}$ of the emitted electron. While we have assumed that photon is incident along the direction normal to the sample surface in the present theoretical study, we also performed simulations of I_{CD} for different values of angle of incidence (not shown for the sake of brevity). It is found that although the individual photointensity for RCP and LCP light vary with angle of incidence, the CD pattern remains unchanged. The incident angle does not have any significant influence on the energy at which CD sign flip occurs either

Various explanations have been proposed for the microscopic origin of the circular dichroism.[12,13,15] But those interpretations do not consider the photon energy dependence of CD-ARPES. Our novel finding shows that not only the spin-texture but also the knowledge of electronic structure and initial-state form factors are required to explain the CD spectra of topological insulators. The initial-state form factors are in turn derived from the total wave function of the electronic states. The initial-state wave function is coupled to the free electron final state via electron-photon coupling and certain values of the magnetic quantum number are selected due to the dipole selection rule. The free electron final state can be expanded in terms of the spherical Bessel function of order l. These Bessel functions when coupled to the initial-state wave functions and modulated by the structure factor $e^{i\mathbf{k_f}\cdot\mathbf{R_i}}$ plays a crucial role in determining the sign of the CD as a function of photon energy. Thus, here we point out the essential quantities required to describe the photon-energy dependence of CD ARPES, which have been neglected so far.[13,15] We find that the chirality of the spin texture of the initial electronic states is masked by the photon-energy-dependent transition matrix element. Our studies provide a way to better understand the response of circularly polarized light in spin-orbit coupled systems.

IV. CONCLUSION

In this work we presented systematic photon-energy-dependent circular polarization response of photoelectrons in ARPES revealing an anomalous behavior of the CD signal on the topological insulator surfaces. Our experimental results supported by our theoretical calculations suggest that measured CD response not only depends on the orbital/spin angular momentum of the initial states but also on the photon energy sampled, mixed-orbital content, and the details of the coupling mechanism of the initial state to the electric field of the incident light. Our experimental findings reveal a rich response behavior of topological surface states thus open new avenues in understanding and controlling topological insulator properties with polarized light.

ACKNOWLEDGMENTS

This work was primarily supported by DARPA Meso Grant No. N66001-11-1-4110. The use of Synchrotron Radiation Center (SRC) was supported by NSF DMR-0537588 under the external user agreement. We acknowledge Peter Riseborough and Luca Perfetti for discussions. T.D. at LANL acknowledges support from Department of Energy, Office of Basic Energy Sciences, Division of Material Sciences. M.Z.H. acknowledges Visiting Scientist support from LBNL and partial support from NSF/DMR-1006492 and A.P. Sloan Foundation.

*Author to whom correspondence and requests for materials should be addressed: mzhasan@princeton.edu

[1] M. Z. Hasan and J. E. Moore, Ann. Rev. Cond. Matt. Phys. **2**, 55 (2011).
[2] J. E. Moore, Nature (London) **464**, 194 (2010).
[3] M. Z. Hasan and C. L. Kane, Rev. Mod. Phys. **82**, 3045 (2010).
[4] X.-L. Qi and S.-C. Zhang, Rev. Mod. Phys. **83**, 1057 (2011).
[5] D. Hsieh, D. Qian, L. Wray, Y. Xia, Y. S. Hor, R. J. Cava, and M. Z. Hasan, Nature (London) **452**, 970 (2008).
[6] Y. Xia, D. Qian, D. Hsieh, L. Wray, A. Pal, H. Lin, A. Bansil, D. Grauer, Y. S. Hor, R. J. Cava, and M. Z. Hasan, Nature Phys. **5**, 398 (2009).
[7] S.-Y. Xu, Chang Liu, N. Alidoust, M. Neupane, D. Qian, I. Belopolski, J. D. Denlinger, Y. J. Wang, H. Lin, L. A. Wray, G. Landolt, B. Slomski, J. H. Dil, A. Marcinkova, E. Morosan, Q. Gibson, R. Sankar, F. C. Chou, R. J. Cava, A. Bansil and M. Z. Hasan, Nature Commun. **3**, 1192 (2012).
[8] D. Hsieh, Y. Xia, D. Qian, L. Wray, F. Meier, J. H. Dil, J. Osterwalder, L. Patthey, A. V. Fedorov, H. Lin, A. Bansil, D. Grauer, Y. S. Hor, R. J. Cava, and M. Z. Hasan, Phys. Rev. Lett. **103**, 146401 (2009).
[9] S. Raghu, S. B. Chung, X.-L. Qi, and S.-C. Zhang, Phys. Rev. Lett. **104**, 116401 (2010).
[10] J. Wunderlich, B.-G. Park, A. C. Irvine, L. P. Zrbo, E. Rozkotov, P. Nemec, V. Novk, J. Sinova, and T. Jungwirth, Science **330**, 1801 (2010).
[11] P. Hosur, Phys. Rev. B **83**, 035309 (2011).
[12] Y. Ishida, H. Kanto, A. Kikkawa, Y. Taguchi, Y. Ito, Y. Ota, K. Okazaki, W. Malaeb, M. Mulazzi, M. Okawa, S. Watanabe, C.-T. Chen, M. Kim, C. Bell, Y. Kozuka, H. Y. Hwang, Y. Tokura, and S. Shin, Phys. Rev. Lett. **107**, 077601 (2011).

[13]S. R. Park, J. Han, C. Kim, Y. Y. Koh, C. Kim, H. Lee, H. J. Choi, J. H. Han, K. D. Lee, N. J. Hur, M. Arita, K. Shimada, H. Namatame, and M. Taniguchi, Phys. Rev. Lett. **108**, 046805 (2012).

[14]J.-H. Park, C. H. Kim, J.-W. Rhim, and J. H. Han, Phys. Rev. B **85**, 195401 (2012).

[15]Y. H. Wang, D. Hsieh, D. Pilon, L. Fu, D. R. Gardner, Y. S. Lee, and N. Gedik, Phys. Rev. Lett. **107**, 207602 (2011).

[16]J. W. McIver, D. Hsieh, H. Steinberg, P. Jarillo-Herrero, and N. Gedik, Nature Nano. **7**, 96 (2012).

[17]Y. Wang and N. Gedik, Phys. Status Solidi RRL **7**, 64 (2013).

[18]S.-Y. Xu, L. A. Wray, Y. Xia, R. Shankar, A. Petersen, A. Fedorov, H. Lin, A. Bansil, Y. S. Hor, D. Grauer, R. J. Cava, and M. Z. Hasan, arXiv:1007.5111v1.

[19]M. Neupane, S.-Y. Xu, L. A. Wray, A. Petersen, R. Shankar, N. Alidoust, Chang Liu, A. Fedorov, H. Ji, J. M. Allred, Y. S. Hor, T.-R. Chang, H.-T. Jeng, H. Lin, A. Bansil, R. J. Cava, and M. Z. Hasan, Phys. Rev. B **85**, 235406 (2012).

[20]S. V. Eremeev, G. Landolt, T. V. Menshchikova *et al*., Nature Commun. **3**, 635 (2011).

[21]R. Denecke, J. Morais, R. X. Ynzunza, G. H. Fecher, J. G. Menchero, J. Liesegang, J. Kortright, Z. Hussain, and C. S. Fadley, Phys. Rev. B **65**, 245421 (2002).

[22]R. X. Ynzunza, H. Daimon, F. J. Palomares, E. D. Tober, Z. Wang, F. J. Garcia de Abajo, J. Morais, R. Denecke, J. B. Kortright, Z. Hussain, M. A. Van Hove, and C. S. Fadley, J. Electron. Spectrosc. Relat. Phenom. **106**, 7 (2000).

[23]R. Schellenberg, E. Kisker, A. Fanelsa, F. U. Hillebrecht, J. G. Menchero, A. P. Kaduwela, C. S. Fadley, and M. A. Van Hove, Phys. Rev. B **57**, 14310 (1998).

[24]U. Heinzman and J. Hugo Dil, J. Phys.: Condens. Matter **24**, 173001 (2012).

[25]H. Mirhosseini and J. Henk, Phys. Rev. Lett. **109**, 036803 (2012).

[26]M. R. Scholz, J. Sánchez-Barriga, J. Braun, D. Marchenko, A. Varykhalov, M. Lindroos, Yung Jui Wang, Hsin Lin, A. Bansil, J. Minár, H. Ebert, A. Volykhov, L. V. Yashina, and O. Rader, Phys. Rev. Lett. **110**, 216801 (2013).

[27]Huiwen Ji, J. M. Allred, M. K. Fuccillo, M. E. Charles, M. Neupane, L. A. Wray, M. Z. Hasan, and R. J. Cava, Phys. Rev. B **85**, 201103(R) (2012).

[28]Zhi Ren, A. A. Taskin, Satoshi Sasaki, Kouji Segawa, and Yoichi Ando, Phys. Rev. B **82**, 241306(R) (2010).

[29]S. Jia, H. Beidenkopf, Ilya Drozdov, M. K. Fuccillo, J. Seo, J. Xiong, N. P. Ong, Ali Yazdani, and R. J. Cava, Phys. Rev. B **86**, 165119 (2012).

[30]J. Xiong, A. C. Petersen, D. Qu, R. J. Cava, and N. P. Ong, Physica E **44**, 917 (2012).

[31]L. Fu, Phys. Rev. Lett. **103**, 266801 (2009).

[32]M. S. Bahramy, P. D. C. King, A. de la Torre, J. Chang, M. Shi, L. Patthey, G. Balakrishnan, Ph. Hofmann, R. Arita, N. Nagaosa, and F. Baumberger, Nature Commun. **3**, 1159 (2012).

[33]C. Jozwiak, C.-H. Park, K. Gotlieb, C. Hwang, D.-H. Lee, S. G. Louie, J. D. Denlinger, C. R. Rotundu, R. J. Birgeneau, Zahid Hussain, and A. Lanzara, Nature Phys. **9**, 293 (2013).

[34]Z.-H. Zhu, C. N. Veenstra, G. Levy, A. Ubaldini, P. Syers, N. P. Butch, J. Paglione, M. W. Haverkort, I. S. Elfimov, and A. Damascelli, Phys. Rev. Lett. **110**, 216401 (2013).

[35]L. A. Wray, M. Neupane, S.-Y. Xu, Y.-Q. Xia, A. V. Fedorov, H. Lin, S. Basak, A. Bansil, Y. S. Hor, R. J. Cava, and M. Z. Hasan, arXiv:1206.1087.